HHS Public Access

Author manuscript

Sci Transl Med. Author manuscript; available in PMC 2024 March 11.

Published in final edited form as:

Sci Transl Med. 2023 October 11; 15(717): eadg1485. doi:10.1126/scitranslmed.adg1485.

Regeneration of neuromuscular synapses after acute and chronic denervation by inhibiting the gerozyme 15-prostaglandin dehydrogenase

Mohsen A. Bakooshli[1,†], **Yu Xin Wang**[1,2,†,*], **Elena Monti**[1], **Shiqi Su**[1], **Peggy Kraft**[1], **Minas Nalbandian**[1], **Ludmila Alexandrova**[3], **Joshua R. Wheeler**[4,5], **Hannes Vogel**[4,5], **Helen M. Blau**[1,*]

[1]Baxter Laboratory for Stem Cell Biology, Department of Microbiology and Immunology, Stanford University School of Medicine, Stanford, CA 94305, USA.

[2]Center for Genetic Disorders and Aging, Sanford Burnham Prebys Medical Discovery Institute, La Jolla, CA 92037, USA.

[3]Vincent Coates Foundation Mass Spectrometry Laboratory, Stanford University, Stanford, CA 94305, USA.

[4]Department of Pathology, Stanford University, Stanford, CA 94305, USA.

[5]Department of Neuropathology, Stanford University, Stanford, CA 94305, USA.

Abstract

To date, there are no approved treatments for the diminished strength and paralysis that result from the loss of peripheral nerve function due to trauma, heritable neuromuscular diseases, or aging. Here, we showed that denervation resulting from transection of the sciatic nerve triggered a marked increase in the prostaglandin-degrading enzyme 15-hydroxyprostaglandin dehydrogenase (15-PGDH) in skeletal muscle in mice, providing evidence that injury drives early expression of this aging-associated enzyme or gerozyme. Treating mice with a small-molecule inhibitor of 15-PGDH promoted regeneration of motor axons and formation of neuromuscular synapses leading to an acceleration in recovery of force after an acute nerve crush injury. In aged mice with chronic denervation of muscles, treatment with the 15-PGDH inhibitor increased motor neuron viability and restored neuromuscular junctions and function. These presynaptic changes synergized with previously reported muscle tissue remodeling to result in a marked increase in

[*]Corresponding author. hblau@stanford.edu (H.M.B.); wwang@sbpdiscovery.org (Y.X.W.).
[†]These authors contributed equally to this work.

Author contributions: M.A.B., Y.X.W., and H.M.B. conceived and designed the experiments and wrote the manuscript. M.A.B., Y.X.W., E.M., S.S., P.K., and M.N. performed the experiments and analyzed the data. L.A. performed the LC-MS/MS experiments and analysis. J.R.W. and H.V. provided the human muscle tissues, diagnostic expertise, and clinical insights. All authors discussed the results and commented on the manuscript.

Competing interests: M.A.B., Y.X.W., and H.M.B. are named inventors on patent application 63/257,264, “A method to restore neuromuscular junction morphology” assigned to Stanford University. H.M.B. is named inventor on patent applications 62/860,180, “Targeting PGE2 degrading enzyme to ameliorate muscle wasting and augment strength”; 62/883,025,“Rejuvenation of aged tissues by inhibition of the PGE2 degrading enzyme, 15-PGDH”; and 63/105,182, “Elevation of mitochondrial biogenesis and function by inhibition of prostaglandin degrading enzyme 15-PGDH” assigned to Stanford University regarding PGDHi licensed to Epirium Bio. H.M.B. is a cofounder, receives consulting fees, and has equity in Epirium Bio. The other authors declare that they have no competing interests.

the strength of aged muscles. We further found that 15-PGDH aggregates defined the target fibers that are histopathologic hallmarks of human neurogenic myopathies, suggesting that the gerozyme may be involved in their etiology. Our data suggest that inhibition of 15-PGDH may constitute a therapeutic strategy to physiologically boost prostaglandin E2, restore neuromuscular connectivity, and promote recovery of strength after acute or chronic denervation due to injury, disease, or aging.

INTRODUCTION

When skeletal muscles lose innervation, they atrophy and weaken. Denervation can result from trauma or neuromuscular wasting diseases such as spinal muscular atrophy (SMA) or amyotrophic lateral sclerosis (ALS). Denervation also occurs with muscle disuse or in advanced age, leading to muscle atrophy and ultimately sarcopenia. Such debilitating reductions in strength affect up to 5% of the population, and health care costs are estimated at 380 billion dollars annually in the United States (1, 2). To date, there are no approved treatments that promote motor axon regeneration and restore neuromuscular connectivity and strength.

Mobility and strength rely on peripheral motor neurons that relay signals from the central nervous system to skeletal muscles. Motor neurons originate in the spinal cord and extend to the skeletal muscles, where they branch to innervate multiple myofibers. Each multinucleated myofiber is contacted by a single motor axon at a synapse known as the neuromuscular junction (NMJ). Although only a small fraction of the myofiber surface area is occupied by its NMJ, the high concentration of acetylcholine receptors (AChRs) at the NMJ suffices to generate the action potentials that drive muscle contraction. Localized signaling through agrin, low-density lipoprotein receptor–related protein 4, receptor associated protein of the synapse, docking protein 7, and muscle-associated receptor tyrosine kinase (MuSK) is necessary for the development and maintenance of the intricate structure of the NMJ and clusters of AChR on postsynaptic myofibers (3–9). With aging, synaptic changes accumulate that underlie age-related defects in muscle innervation (10–12). Metabolic changes in energy utilization, autophagy, and nutrition have all been implicated in the progressive loss of neuromuscular synapse morphology and function in aged mice (10, 13, 14). Despite this knowledge of NMJ structure and function, therapeutic interventions that promote reinnervation and restore neuromuscular synapses after damage or in aging are lacking.

We previously demonstrated that prostaglandin E2 (PGE2) is required for muscle stem cell proliferation and efficacious muscle regeneration after injury (15). More recently, we found that the PGE2-degrading enzyme 15-prostaglandin dehydrogenase (15-PGDH) accumulates with age (16). When 15-PGDH is overexpressed in muscles of young mice, they atrophy and weaken within 1 month, recapitulating the effect of years of aging. We therefore designated 15-PGDH a gerozyme, a molecular determinant of muscle wasting that increases with aging. When 15-PGDH activity is inhibited pharmacologically in aged mice, PGE2 concentrations increase twofold and are restored to amounts seen in young mice, leading to an increase in muscle strength (16). Mechanistically, this rejuvenation of muscle function is due to

the induction of muscle mitochondrial biogenesis and reduction in expression of ubiquitin ligases responsible for muscle atrophy, termed atrogenes, and transforming growth factor–β (TGFβ) signaling. Together, these data showed that modulation of PGE2 abundance to a physiologic range of young muscle markedly affects muscle strength. However, these studies did not identify a biological driver of 15-PGDH expression with aging.

Here, we tested the hypothesis that loss of innervation triggered the expression of 15-PGDH in muscle. We found that expression of the gerozyme increased markedly in young mouse muscles after surgically or injury-induced denervation. Pharmacological inhibition of 15-PGDH promoted formation of NMJs and accelerated recovery of force after peripheral nerve crush injury in young mice. In aged mice, 1 month of 15-PGDH inhibition (PGDHi) reversed age-related NMJ loss of structure and function, leading to increased force generation. Mechanistically, increasing PGE2 concentrations by PGDHi or intramuscular delivery of PGE2 activated the cyclic adenosine monophosphate (cAMP) response element–binding protein (CREB) in spinal cord motor neurons, providing evidence that this metabolite acts not only on muscle but also on neurons to promote axon regeneration and survival. In human tissues, we detected 15-PGDH aggregates in discrete foci that comprise the “bulls-eye” of target fibers (17), a hallmark of diverse human neurogenic myopathies, which suggests that 15-PGDH may play a role in these muscle wasting diseases. Furthermore, 15-PGDH can be pharmacologically targeted using a small-molecule compound [SW033291 (SW)] to regenerate motor axons, restore muscle innervation, and augment formation of NMJs after either acute denervation due to injury or chronic denervation due to aging, leading to increased muscle strength. These data highlight 15-PGDH as a molecular effector of denervation in myofibers. Together, our findings suggest that inhibition of the gerozyme 15-PGDH may have therapeutic potential to restore neuromuscular connectivity and overcome loss of muscle strength due to trauma, neuromuscular wasting diseases, or aging.

RESULTS

15-PGDH expression and activity are induced by muscle denervation

We previously showed that increased 15-PGDH expression in myofibers caused the muscle wasting and weakness that occurs with aging (16). When 15-PGDH was ectopically expressed in young adult mouse muscles, they atrophied within 1 month. Because structural alterations in neuromuscular synapses and partial denervation of myofibers are hallmarks of skeletal muscle aging (10), we hypothesized that NMJ dysfunction plays a causal role in 15-PGDH expression.

To determine whether myofiber denervation leads to increased 15-PGDH abundance, we severed the connection between lumbar motor neurons and the skeletal muscles of the hind limb, including the extensor digitorum longus (EDL), tibialis anterior (TA), gastrocnemius (GA), and soleus (Sol), by transecting the sciatic nerve. We performed unilateral sciatic nerve transection (SNT), removing 5 mm of the sciatic nerve of one leg in young mice and leaving the nerve in the contralateral leg intact as a control. We assayed the effect of denervation on myofibers 14 days after SNT (Fig. 1A). Reinnervation after SNT did not occur within the time span of this experiment and was confirmed by 3D

morphologic immunofluorescence analyses of NMJs in whole mounts of myofiber bundles dissected from the EDL muscle, a small muscle that is amenable to this type of analysis. Innervation of NMJs was confirmed in contralateral EDL muscles by the colocalization of the axonal marker, neurofilament (NF) protein, with bungarotoxin (BTX), a snake venom toxin that binds AChRs on the postsynaptic myofiber sarcolemma (Fig. 1B, left). BTX staining revealed that AChRs persist on the postsynaptic myofibers even in the absence of innervation, which was confirmed by the absence of NF staining in the denervated EDL muscles 14 days after SNT (Fig. 1B, right).

We then determined whether 15-PGDH abundance increased after muscle denervation. Using multiplex proteomic tissue imaging [codetection by indexing (CODEX)], we observed a marked increase in 15-PGDH protein in the denervated myofibers of the TA muscle 14 days after SNT (Fig. 1C and fig. S1, A and B). CODEX enables localization of up to 40 proteins simultaneously in diverse cell types within tissue sections by immunofluorescence (18). This is achieved by using antibodies conjugated to unique oligonucleotides that are visualized after reversible hybridization with complementary oligonucleotides conjugated to fluorophores. CODEX overcomes tissue autofluorescence and background, which can be problematic in discriminating authentic from artifactual signal in damaged or aged muscles (19). In contrast to the robust staining of NF protein in the axons of motor neurons innervating the contralateral muscles, NF protein staining in transverse sections of the nerve tracts of denervated TAs was not detectable, confirming the efficacy of SNT (Fig. 1C, insets). CODEX analysis revealed extensive infiltration of immune cells in denervated TAs at this time point, whereas the vasculature was not affected by SNT (fig. S1A). In agreement with our histological findings, we observed a 20-fold increase in 15-PGDH (*Hpgd*) mRNA in a published RNA sequencing (RNA-seq) time course of denervated mouse muscle (Fig. 1D) (20), a fourfold increase in protein abundance, and enzymatic activity in the GA muscles by Western blot analysis of denervated legs after SNT (Fig. 1E and fig. S1C), compared with contralateral controls. A 2.5-fold increase in *Hpgd* compared with wild-type controls was also seen with chronic denervation in the SMNΔ7 mouse model of SMA (21), a heritable motor neuron disease (fig. S1D).

15-PGDH is the rate-limiting enzyme in the degradation of PGE2 to 13,14-dihydro-15-keto-PGE2 (PGEM) (22, 23). We found that in accordance with the increase in protein, 15-PGDH enzyme–specific activity was increased in the protein lysates of denervated GA muscles compared with contralateral controls (Fig. 1F). This resulted in an increase in the PGE2 breakdown product, PGEM, detected using a highly sensitive liquid chromatography with tandem mass spectrometry (LC-MS/MS) method that distinguishes closely related prostaglandins and their metabolites (Fig. 1G and fig. S1E) (16). Together, these findings demonstrated that denervation induces *Hpgd* expression in myofibers and a marked increase in enzyme abundance and activity.

Denervation drives the increase in 15-PGDH abundance in aged muscle

We sought to determine whether denervation plays a role in the increase in 15-PGDH expression seen with aging (16). Denervation is known to progressively increase with aging, and the larger fast motor units responsible for rapid force generation are more

susceptible to denervation than slow motor units (24, 25). Specifically, muscles composed of predominantly fast-twitch glycolytic type IIb myofibers undergo higher rates of denervation than slow-twitch oxidative type I and IIa myofibers with aging (26). Thus, we hypothesized that the expression of 15-PGDH would differ in accordance with the fiber-type composition and denervation status of aged muscles. To test this possibility, we assessed the extent of denervation across slow- and fast-twitch muscle groups by immunofluorescence microscopy and 15-PGDH abundance by Western blot analysis for young and aged mice (Fig. 2, A to C). We scored denervation in the primarily fast-twitch EDL (fig. S2A, right) and the primarily slow-twitch Sol (fig. S2A, left) muscles, both of which are smaller muscles amenable to whole-mount analysis. In agreement with previous reports (10, 27), we found that 20.2 ± 2.9% of myofibers in the aged EDL muscle are denervated, assessed by an absence of NF and the synaptic vesicle protein 2 (SV2) staining at postsynaptic AchRs, compared with 4.4 ± 1.5% in young EDL muscles (Fig. 2, A and B). By contrast, slow motor units of aged Sol myofibers do not exhibit an increase in denervation at 24 months (Fig. 2B). 15-PGDH protein abundance determined by Western blot analysis increased with age in accordance with the proportion of fast myofibers in each muscle group (Fig. 2C and fig. S2B). In aged EDL muscles, which are composed of mostly fast motor units and are the most severely denervated muscles of those analyzed, 15-PGDH protein abundance was increased more than five-fold in aged compared with young mice (Fig. 2C and fig. S2B). By contrast, in aged Sol muscles, composed of slow myofibers, no increase in 15-PGDH abundance was observed with age.

To determine whether 15-PGDH protein expression correlated with fiber types in aged muscles, we assessed the spatial distribution of 15-PGDH in fast- and slow-twitch myofiber types. For this purpose, we focused on the GA muscles that have a mixed fiber-type composition and exhibit an intermediate increase in 15-PGDH levels with aging. Denervation of the GA is known to occur along the skin-to-bone axis (28), with denervation occurring first in the fast glycolytic type IIb myofibers in superficial regions close to the skin and later in the slow oxidative type I and IIa myofibers in deeper regions close to the bone (Fig. 2D, top). 15-PGDH is not detectable by CODEX in young GA myofibers (16). However, a notable localized expression of 15-PGDH was apparent in aged GA muscle that was restricted to type IIb myofibers in superficial regions (Fig. 2D, bottom), in accordance with the known aging-associated denervation of fast motor units (10, 27). Thus, at single-myofiber resolution in the GA muscle, 15-PGDH protein accumulates in fast-twitch myofibers that become progressively denervated with age. These findings suggested that the chronic neuropathic alterations at the NMJs and loss of innervation of myofibers that occur with aging may drive 15-PGDH expression in aged muscle.

15-PGDH is part of a distinct genetic program that is triggered by denervation and sustained over time

To gain mechanistic insights into the molecular and cellular regulation of 15-PGDH by denervation, we performed single-nucleus RNA-seq (snRNA-seq) using GA muscles from mice subjected to unilateral SNT (Fig. 3A). Single-cell RNA-seq is not suited to studies of skeletal muscle because myofibers are syncytial cells composed of myonuclei with transcriptional heterogeneity (29, 30). For this reason, we isolated single nuclei using

fluorescence-activated cell sorting from which we generated barcoded cDNA libraries for sequencing using the 10X Chromium system. We profiled transcriptomes from 13,888 single nuclei from control and denervated muscles. Using unbiased clustering, we were able to distinguish all major cell types expected in skeletal muscle, including myonuclear subtypes found at NMJs and myotendinous junctions (MTJs), muscle stem cells, fibroadipogenic progenitors (FAPs), endothelial cells, immune cells, smooth muscle cells, adipocytes, tenocytes, and pericytes (Fig. 3B and fig. S3, A to D).

The most apparent change in cell-type composition in denervated muscles was a new and predominant population of reprogrammed “denervated myonuclei” (DN myonuclei) (Fig. 3C and fig. S3C). DN myonuclei expressed *Hpgd* in contrast to innervated myonuclei (Fig. 3D and fig. S3E). DN myonuclei are distinct from specialized subsynaptic NMJ myonuclei and MTJ myonuclei, neither of which expressed *Hpgd*. In contrast, immune cells, which increased somewhat in abundance in agreement with our CODEX analysis (Fig. 3C and fig. S1A), and tenocytes expressed *Hpgd* irrespective of innervation status (Fig. 3D). *Hpgd*-expressing myonuclei expressed low levels of genes encoding beneficial metabolic functions like mitochondrial enzymes (Fig. 3E, bottom), the voltage-dependent anion channel (*VDAC1*) and mitochondrial glycolytic enzyme pyruvate dehydrogenase (*PDHA1*) (Fig. 3F). Conversely, myonuclei that expressed *Hpgd* also exhibited genomic (31, 32), metabolic, and catabolic stress responses such as p53 signaling, cellular senescence, FoxO signaling, TGFβ signaling, and autophagy (Fig. 3E, top). Moreover, DN myonuclei exhibited increased expression of the autophagosome membrane protein LC3A (*Map1lc3a*) and the mitophagy regulator Parkin (*Prkn*) (Fig. 3G) that are often associated with mitochondrial damage and destruction. Together, these findings demonstrated that myofibers were the main source of 15-PGDH in denervated muscles and established denervation as a driver of 15-PGDH expression in myonuclei that are undergoing genomic and metabolic stress responses.

To establish the temporal dynamics of *Hpgd* expression after denervation, we analyzed a 3-month time course of gene expression changes after SNT (20) and found that the expression pattern of *Hpgd* (early and persistent) after denervation was distinct from that of other well-known hallmarks of denervation: inflammatory (immediate), catabolic (early and transient), and extracellular matrix remodeling (late) genes (Fig. 3, H and I). *Hpgd* increased markedly 3 days after denervation and continued to increase, reaching 10-fold and ~20-fold that detected in contralateral control leg muscles on days 14 and 90, respectively (Fig. 3H, blue line; Fig. 1D). *Hpgd* displayed a distinct temporal expression pattern from other genes known to cause muscle protein degradation: ubiquitin ligases, termed atrogenes, and the TGFβ family member myostatin (*Mstn*). In contrast to *Hpgd* that is highly expressed and sustained at 90 days, expression of atrogenes transiently increases at day 3 and rapidly declines at days 7 and 14 after SNT. *Mstn* expression does not increase but instead rapidly declines at day 7 after SNT (fig. S4, A and B, and data file S1). Other genes that share the same expression dynamic as *Hpgd* are associated with anoikis, a form of cell death (Fig. 3I, blue) and stress-associated genes like peptidyl-lysine deacetylation including histone deacetylase 4 (*HDAC4*), a class IIa HDAC that promotes neurogenic muscle atrophy by inducing the degradation of myosins, peroxisome proliferator-activated receptor-gamma coactivator 1 alpha (PGC-1α), and chaperones (33, 34). These data provided molecular

support for our previous functional findings in aged mice showing that inhibition of 15-PGDH had pleiotropic beneficial effects in countering muscle atrophy, culminating in an increase in strength (16).

15-PGDH aggregation denotes target fibers, histopathologic hallmarks of chronic nerve damage in human neurogenic myopathies

Severe human muscle wasting disorders often arise from chronic nerve damage and present with a histopathological diagnosis of “target” or “targetoid” fibers (17, 35, 36). These fibers are characterized histochemically by a central bullseye pattern evident by reduced form of nicotinamide adenine dinucleotide (NADH)–tetrazolium reductase staining, indicative of the absence of mitochondria. They are also characterized by an accumulation of the autophagosome marker LC3. The presence of target fibers is a clinical indication of muscles undergoing denervation with signs of reinnervation (37). Frequently, patients present with weakness that is associated with partial or complete denervation in conjunction with muscle atrophy, including SMA type 3, ALS, and nerve root compression injuries (lumbar radiculopathy) (38, 39).

We hypothesized that 15-PGDH protein accumulation was associated with target fibers in human myopathies. We obtained biopsies ($n = 10$) from patients with neurogenic myopathies and performed histological and immunofluorescence analysis for 15-PGDH, autophagy, and mitochondrial markers. The 10 biopsies analyzed were from patients who encompassed a range of etiologies including axonal neuropathies, myositis, and motor neuron disease. Using serial sections, we performed classic NADH staining of target fibers and confirmed that the central targets are devoid of NADH in accordance with the lack of mitochondria in these regions. In 9 of the 10 samples, we found that the target was composed, at least in part, of 15-PGDH aggregates (Fig. 4A). The one exception was a biopsy from a patient with a drug toxicity–induced neuropathy in which staining patterns for mitochondria were complex and target fibers could not be confidently distinguished. 15-PGDH aggregates were detected in some myofibers that did not exhibit classical NADH-negative targets, suggesting that 15-PGDH aggregation may precede mitochondrial depletion and that 15-PGDH may constitute a marker for detecting these targets. We analyzed the expression of LC3A and found that it was colocalized with 15-PGDH in the targets (Fig. 4B, left and middle panels), whereas mitochondrial protein pyruvate dehydrogenase (PDHA) was excluded from these central regions (Fig. 4B, right). These histological observations were absent in muscle biopsies from healthy patients (fig. S5, A and B). Collectively, our data provided evidence that 15-PGDH was colocalized with autophagy-associated gene products in regions lacking metabolic function in denervated myofibers, supporting the snRNA-seq data for denervated mouse muscles after SNT (Fig. 3). These data suggested 15-PGDH immunostaining as a histopathologic marker of target fibers and provided additional evidence in support of a role for 15-PGDH aggregates in the pathogenesis of human neurogenic myopathies.

15-PGDHi induces NMJ and motor axon regeneration and accelerates recovery from nerve crush injury

We postulated that PGDHi could promote regeneration of the motor axons that innervate the muscle after peripheral nerve injury. To test this hypothesis, we performed unilateral sciatic nerve crush (SNC) in young healthy mice. In contrast to SNT, crush injuries do not sever the endoneural tubes along which axons regrow, and the damage can therefore be repaired. Spontaneous regeneration and the recovery of innervation without treatment occurs over about 50 days (40).

To determine whether regeneration was accelerated by PGDHi, SNC-injured mice were treated daily intraperitoneally with a small-molecule inhibitor specific to 15-PGDH (SW; PGDHi) or vehicle (Fig. 5A). To assess neuromuscular connectivity over a time course of days postinjury (dpi), we electrically stimulated the tibial nerve and measured the force generated by the muscle contractions in live mice. To ensure that force measurements resulted from nerve excitation, electrodes were located proximal to the tibial nerve, distal to the crush injury, and the current was adjusted to a threshold sufficient for nerve activation but not muscle fiber depolarization (see Materials and Methods). As expected, SNC led to a progressive loss of force. Nerve stimulation in the crushed legs revealed a drop in force to 34 ± 2.8% of that generated by uninjured contralateral legs by 3 dpi, which was further reduced to 21 ± 1.5% by 7 dpi (Fig. 5B and fig. S6, A to C). We observed no significant difference between PGDHi- and vehicle-treated experimental groups. This finding indicates that the sciatic nerve injury was robust and resulted in a degenerative phase during the first week after injury in both vehicle- and PGDHi-treated groups that culminated in ~80% reduction in force assessed as plantar flexion torque, which reflects the extensive denervation of myofibers after SNC as reported previously by others (41).

By 14 dpi, we observed a 37.2 ± 4.9% increase in the tetanic force generated by muscles of PGDHi-treated mice relative to vehicle-treated controls, indicative of an acceleration in recovery from nerve crush damage (Fig. 5B and fig. S6, A to C). The increase in force during this regenerative phase was not due to a change in body weight (fig. S6D). To determine whether the increase in force was due to an increase in muscle mass, we measured the weight of Sol and GA muscles, the primary muscles responsible for plantar flexion force generation. Although an increase in muscle mass (6.1 ± 1.7%) was observed in injured legs at 14 dpi (Fig. 5C), the increase in specific force (32.2 ± 4.1%) compared with vehicle-treated mice after injury (Fig. 5D) exceeded the increase in muscle mass. This finding suggested that the contractile function of the muscle was increased and that this increase was due to enhanced innervation. By contrast, uninjured contralateral legs exposed to vehicle or PGDHi exhibited no significant change in tetanic force or muscle mass at 14 dpi (fig. S6, A, C, and E).

Reinnervation after SNC injury requires the regeneration of motor axons and the formation of NMJs. To confirm the effect of PGDHi on muscle reinnervation, we performed histological analysis of the sciatic nerve and the muscle and assessed the extent of axon regeneration and NMJ formation. To quantify the degree of axon regeneration, we scored the number of motor axons in the sciatic nerve distal to the injury site. Sciatic nerves were collected for histological assessment, and motor axons were identified by

immunofluorescence staining for NF and choline acetyltransferase (ChAT). We trained a neural network model to identify and quantify motor axons ($ChAT^+$ NF^+), other axons ($ChAT^-$ NF^+), and blood vessels in micrographs of sciatic nerve cross sections. This allowed us to quantify axons in sciatic nerves of uninjured and 14-dpi legs (Fig. 5E and fig. S6F). As expected, injured nerves contained fewer axons overall (Fig. 5F). The sciatic nerves after SNC of mice treated with PGDHi contained 1.9-fold more motor axons (797 ± 69.3) compared with vehicle-treated control mice (415.2 ± 52.5). This represents 76.3% (PGDHi-treated) and 39.7% (vehicle-treated) of the number of motor axons found in uninjured sciatic nerves (1045.1 ± 55), respectively (Fig. 5F, left). Treatment with PGDHi did not affect the number of other axons (Fig. 5F, right), which suggested that the regenerative effect was specific to motor neurons.

To quantify the reestablishment of neuromuscular synapses, we quantified the innervation status of NMJs. This was achieved by assessing the coincidence of presynaptic motor neuron staining with antibodies to NF and SV2 and postsynaptic AChR marked by BTX in the injured legs compared with uninjured contralateral legs 14 dpi. In accordance with previous studies (42, 43), partial recovery of innervation was observed in vehicle-treated controls at 14 dpi. Pharmacological inhibition of 15-PGDH increased innervation in injured EDL muscles from 84.5 ± 2.2% in vehicle-treated controls to 97.4 ± 2.1% in PGDHi-treated mice (Fig. 5, G and H). These findings indicated that reinnervation and NMJ formation were markedly increased, indicative of an accelerated recovery when 15-PGDH was inhibited after peripheral nerve injury. Together, these data suggest that PGDHi enhanced recovery from peripheral nerve injury by promoting nerve regeneration and formation of functional neuromuscular synapses, which led to increased strength (Fig. 5I).

15-PGDHi improves NMJ morphology and increases strength in aged mice

We sought to determine whether PGDHi led to reinnervation of NMJs and restored motor function in aged muscles. Aged mice are chronically denervated because of the progressive loss of NMJs over time (10, 11). We injected aged mice (24 to 26 months) daily intraperitoneally for 1 month with vehicle or PGDHi (Fig. 6A). EDL muscles were immunostained to visualize motor axons and terminals and postsynaptic AChRs at NMJs in whole-mount preparations (Fig. 6B). In agreement with previous reports (10), we observed a high incidence of alterations in NMJs, including denervation (21.6 ± 2.3%), axonal swelling (19.6 ± 1.4%), and postsynaptic AChR fragmentation (28.9 ± 2.8%), in vehicle-treated aged mice (Fig. 6, B to E, and fig. S7). PGDHi reduced the incidence of these NMJ structural abnormalities in aged mouse muscles (Fig. 6, B to E). We postulated that the reduction in myofiber denervation and improvement in NMJ morphology in aged mice upon PGDHi could lead to an increase in muscle mass and motor function. After 1 month of PGDHi treatment, we found that aged mice exhibited an increase in muscle mass and plantar flexion force compared with vehicle-treated controls (Fig. 6, F and G).

We postulated that PGDHi would alter the organization of AChRs and their stability in aged NMJs. We found that AChRs appeared fragmented, and endolysosomal vesicles containing BTX^+ AChR were increased in aged muscles (Fig. 6H), in agreement with findings by others (13). PGDHi restored the morphology of NMJs to pretzel-like structures found in

young EDL muscles and led to a reduction in the number of AChR-rich endolysosomal vesicles at NMJs of aged mice (Fig. 6, H and I). These data demonstrated that PGDHi ameliorated changes to NMJ structure and function in aged mice, leading to increased muscle mass and strength.

PGE2 stimulates CREB in spinal cord motor neurons

To investigate the mechanism underlying the recovery of force observed with PGDHi treatment, we analyzed PGE2 signaling in motor axons. On the basis of our finding that inhibition of 15-PGDH accelerated the regeneration of axons and NMJs after acute damage after SNC and reduced the chronic neuropathic process in aged mice, we hypothesized that PGE2 acted not only on muscle but also on motor neurons. The somata of lower motor neurons that innervate the hind limb muscles reside within the spinal cord of the lumbar vertebrae (Fig. 7, A and B) at a substantial distance from the muscle. We postulated that elevated PGE2 abundance after PGDHi treatment could elicit a pro-regenerative response in lower motor neurons.

We postulated that PGE2 enhanced motor neuron function by signaling via cAMP and phosphorylation of CREB (p-CREB). Several lines of evidence suggest that CREB plays a role in neuron survival and function (44–46). We analyzed a single-cell transcriptomic atlas of mouse spinal cord (47) and found that prostaglandin receptors, particularly the PGE receptor EP4 (*Ptger4*) that signals through cAMP-CREB, was highly expressed in cholinergic neurons (fig. S8A). To test whether PGDHi leads to activation of CREB in motor neurons, we isolated the lumbar spinal cords of mice 14 days after SNC injury and performed immunofluorescence staining to quantify CREB phosphorylation in ChAT-expressing motor neurons. $ChAT^+$ motor neurons (37 ± 2%) had nuclear p-CREB in PGDHi-treated mice compared with 22 ± 3% in vehicle-treated controls (Fig. 7C and fig. S8B). To test whether PGE2 from muscle could suffice to elicit CREB phosphorylation in motor neurons, we injected the GA muscles of aged mice with dimethyl-PGE2 (dmPGE2), which is not degraded by 15-PGDH (48), and assessed p-CREB by immunofluorescence in lumbar motor neurons (Fig. 7D). $ChAT^+$ motor neurons (75 ± 4%) had robust nuclear p-CREB signals 1 hour after PGE2 injection, compared with 30 ± 4% in the phosphate-buffered saline (PBS)–injected mice (Fig. 7E and fig. S8C). Together, these experiments suggested that PGE2 could exert a beneficial effect on motor neurons as a muscle-derived factor. They also confirmed that PGE2 promoted CREB phosphorylation in lumbar motor neurons.

We reasoned that the recovery of strength that we observed in aged mice after PGDHi treatment was due to a protective effect of PGE2 on lumbar motor neurons (49). PGE2-EP4 signaling has been reported to have a neuroprotective effect after cerebral ischemia injury (50). To test whether PGDHi counters the neurodegeneration seen in aged mice, we determined levels of cleaved caspase-3 (Cl-Casp3) (Fig. 7F), a marker of apoptosis seen in motor neurons in ALS (51–53). In contrast to young mice that had no apoptotic motor neurons, we found that aged mice had 11.6 ± 2.5% $Cl\text{-}Casp3^+$ $ChAT^+$ motor neurons (Fig. 7G). After PGDHi treatment, the incidence of $Cl\text{-}Casp3^+$ $ChAT^+$ motor neurons was reduced to 4.2 ± 0.6%, suggesting that increased PGE2 levels prevented motor neuron apoptosis.

PGE2 may constitute a muscle-derived retrograde factor that enhances neuronal function, but PGDHi acts systemically after intraperitoneal delivery, so we cannot rule out that the increase in PGE2 derived from tissues and cell types in addition to muscle. Together, these results revealed that PGE2, either resulting from PGDHi or from intramuscular delivery, can activate CREB in spinal cord motor neurons and mitigate motor neuron apoptosis in aging.

DISCUSSION

When skeletal muscles lose innervation, they atrophy and weaken, which compromises mobility and affects quality of life. Denervation can be sudden due to a traumatic injury that compresses or severs the nerves or can occur progressively over time with disease or age. A total of 3 to 5% of the population in the United States suffers from such disorders, and the available treatment options are limited (1, 2). These data underscore the need for a treatment to increase neuromuscular connectivity and strength. In addition, insights into motor nerve regeneration could potentially inform CNS nerve regeneration (54). In this report, we identified 15-PGDH as a promising therapeutic target for enhancing peripheral neuron regeneration and augmenting neuromuscular function and strength after either an acute loss of innervation due to injury or a chronic loss of innervation due to aging.

Here, we showed that short-term PGDHi using a small-molecule drug promoted motor neuron regeneration. A major advantage of the approach that we describe here is that it entails a physiologic increase in PGE2 brought about by preventing its degradation. Two weeks of exposure to PGDHi resulted in an acceleration in the recovery of innervation and strength after nerve crush injury. PGDHi also restored neuromuscular connectivity in aged mice. The onset of the neuropathology that leads to partial dennervation is first evident at about 18 months of age in the mouse (11), long before the onset of sarcopenia. One month of PGDHi treatment in 24-month-old mice sufficed to ameliorate aging-associated presynaptic axonal swelling, postsynaptic AChR fragmentation, and endolysosomal degradation at NMJs, leading to an increase in strength. A comparable reversal of NMJ loss in aged mice required lifelong caloric restriction or a month of exercise (10), but drug treatments are lacking. Our results highlight the potency of a transient drug treatment, PGDHi, in restoring the connection between the motor neurons and myofibers that is lost either because of acute injury-induced or chronic aging-induced denervation.

We found that PGDHi acts not only on the muscle but also on the neurons that innervate the muscles. The increase in PGE2 resulting from PGDHi accelerated regeneration of damaged axons that extend from lumbar motor neurons in the spinal cord. Moreover, aged motor neuron apoptosis was reduced after PGDHi. Increased PGE2 after systemic PGDHi or direct intramuscular injection of PGE2 elicited cAMP signaling and the rapid accumulation of pCREB in the nuclei of lumbar $ChAT^{+}$ motor neurons after nerve crush injury or in aging, respectively. In agreement, data of others showed that PGE2 promoted neurite outgrowth in vitro in the neuroblastoma hybrid cell line 34 (NSC-34) motor neuron–like cell line in a cAMP-dependent manner (44) and that constitutive activation of CREB promoted axon regeneration in dorsal root ganglion neurons after spinal cord injury in mice in vivo (45). Although we cannot rule out a potential indirect effect of PGE2 on the clearance of debris from damaged axons by macrophages and myelinating Schwann cells

in the recovery from acute nerve injury [reviewed in (55, 56)], this transient inflammatory response cannot account for the reinnervation of NMJs that we observed with PGDH inhibitor treatment in aged mice because axons are not damaged in this pathology. Thus, we uncovered a connection between PGE2 and neuro-regenerative CREB signaling in lumbar motor neurons.

When innervation is lost, electrical activity and calcium signaling decline, glucose uptake is reduced, and myonuclei become reprogrammed to express a series of stress-related and atrophy genes. 15-PGDH (*Hpgd*) gene expression, which causes muscle atrophy (16), is rapidly induced after denervation and then sustained over a 3-month time course. These temporal dynamics differ from the atrophy inducer myostatin and canonical atrogenes, the E2 ligases that degrade muscle proteins, suggesting different mechanisms of regulation for each of these muscle wasting gene programs.

Resolution of the epigenetic regulation of 15-PGDH triggered by denervation may provide further mechanistic insights into its function. One possibility is that the increase in 15-PGDH expression after denervation plays a role in dampening the inflammatory response. An inflammatory gene program is immediately precipitated by nerve injury as part of the body's natural healing mechanism, of which PGE2 is a major component. An increase in 15-PGDH would limit the exposure to PGE2. However, if expression of 15-PGDH is prolonged, then the suppression of PGE2 concentrations will likely not only reduce inflammation but will also reduce beneficial PGE2 signaling to the myofiber and motor neuron, leading to muscle wasting, as occurs in aging. Thus, the temporal control of 15-PGDH expression is crucial to its function and, if protracted, will be deleterious. Elucidation of the mechanisms leading to 15-PGDH expression will be of great interest for understanding how it is controlled in homeostasis and what goes awry in pathological conditions.

Myofiber health and metabolic fitness are known to affect NMJ formation, stability, and signaling integrity (14, 57). After injury, axons regenerate along endoneurial tubes to reinnervate their original synaptic sites, but these synapses will only persist if they are apposed by viable myofibers (40). The stability of AChR on the postsynaptic membrane is critical in mediating this connection. Denervation leads to increased degradation of postsynaptic AChRs by the ubiquitin ligase muscle RING-finger protein-1 (MuRF1; *Trim63*) (58, 59). Disruption of autophagy or autophagosome formation in mouse muscle fibers leads to degradation of postsynaptic AChRs by endocytosis, which causes denervation (13). Conversely, boosting mitochondrial function in mouse myofibers by overexpression of PGC1α increases NMJ stability and maintenance (14). Neuromuscular synapses have also been restored by agonist antibodies against MuSK that prevented neonatal lethality in a mouse model of congenital myasthenia gravis (60). We previously showed that PGDHi reduces the level of MuRF1 and increases autophagy and remodeling of muscle mitochondria morphology, in addition to boosting mitochondrial numbers and gene expression (16). In the present study, we found that PGDHi not only decreases axonal swelling but also reduces the number of $AChR^+$ endocytic vesicles in the muscle, suggesting that the increase in stabilization of the NMJ and neuromuscular function is also mediated by postsynaptic mechanisms that prevent AChR degradation.

The relevance of our findings to human disease is evident from our histopathological analysis of muscle biopsies from patients with neurogenic myopathies. 15-PGDH aggregates comprise the bullseye of fibers long designated by pathologists as targetoid or target fibers. Target fibers are associated with continuous denervation and reinnervation, signs of neurogenic remodeling in patients with muscle pathologies (17). They are observed in a range of motor nerve injuries, such as those arising from axonal neuropathies [including nerve root compression (lumbar radiculopathy), neurogenic amyloidosis, and various etiologies of nerve injuries], myositis, and motor neuron diseases (including ALS and SMA) (17, 37, 38). The molecular nature of these target fibers has long been a matter of debate, but the target regions are thought to be metabolically inactive and devoid of mitochondria, because they lack NADH and adenosine triphosphatase enzymatic activity. Here, we showed that, like fast-twitch myofibers of aged mice, 15-PGDH aggregates together with autophagy component LC3A constitute the core of the bullseye in target fibers in human myopathic conditions. PGDHi treatment inhibits the enzymatic activity of 15-PGDH and is sufficient to reduce motor neuron pathologies after crush injury and in the aged mouse. Although the expression and distribution of the enzyme are not altered, inhibiting its activity overcomes muscle atrophy and increases innervation. These findings implicate 15-PGDH in human neuromuscular wasting pathology and suggest that PGDHi has therapeutic potential in ameliorating diverse heritable and acquired myopathic conditions in patients.

Although data from this study suggest that 15-PGDH expression in denervated myofibers drives atrophy and its inhibition promotes recovery of innervation, there are still limitations and outstanding questions that require further comprehensive studies. Genetic models of muscle-specific deletion of *Hpgd* after nerve injury and aging could better determine the absolute contribution of muscle 15-PGDH in wasting. Moreover, our current understanding of 15-PGDH aggregation in chronic denervation conditions and human neurogenic myopathies is incomplete. Molecular approaches to interrogate this structure and whether this spatial localization contributes to 15-PGDH accumulation could lead to new insights into the cellular physiology of muscle fibers.

In conclusion, PGDHi may represent a tractable and translatable strategy to promote neuromuscular recovery after nerve injury. This strategy benefits from its complementary effects on muscle and the motor neurons to restore their connectivity. Promoting motor axon and NMJ regeneration could potentially be applied to conditions where muscle denervation leads to the loss of strength and function, including acute trauma, nerve compression injuries, chronic neurodegenerative disorders, and motor neuron diseases such as ALS and SMA. Combining this approach with disease-modifying therapies that halt pathological progression could potentially lead to the recovery of neuromuscular function.

MATERIALS AND METHODS

Study design

The study is designed to experimentally test whether denervation leads to myofiber expression of 15-PGDH using surgical transection, crush injury mouse models, and naturally occurring neuropathic progression with aging in mice. Moreover, we aimed to resolve the function of 15-PGDH on the process of innervation using a small-molecule inhibitor

(PGDHi) to block its activity and measure histological changes to NMJs and sciatic nerves and functional changes in neuromuscular connectivity by in vivo force measurements. The selection of day 14 as a time point for analysis and the sample size of surgical models were informed by prior data from published RNA-seq (20) and established rates of denervation and reinnervation (41). Sample sizes were increased in studies involving aged mice to account for the heterogeneity of aging, informed by our prior studies using PGDHi (16). In vivo force measurements after electrically stimulating the tibial nerve allowed us to monitor muscle strength longitudinally, and histological analyses of muscle, sciatic nerve, and spinal cord were performed at day 14 at the earliest stages of reinnervation. Mice were randomized into treatment groups so that each group had an equal distribution of body weight. Histological analyses requiring manual quantification (NMJ analyses) were performed by blinded experts, unblinding after all data were collected. Certain data points lacking information are the result of poor-quality samples (i.e., damaged/incomplete tissues) or technical errors during data collection (i.e., equipment/procedural malfunction). All sample size information for each experiment is indicated in the figure legends and represents biological replicates.

Animal husbandry

All animal experiments and protocols complied with the institutional guidelines of Stanford University and Administrative Panel on Laboratory Animal Care. Male C57BL/6 mice were used in this study. Aged mice (24 to 26 months old) were obtained from the U.S. National Institute on Aging aged colony, and young mice (2 to 4 months old) were purchased from the Jackson Laboratory.

In vivo drug treatment

Aged mice—Mice were treated for 1 month once a day intraperitoneally with SW (5 mg/kg) or vehicle {10% ethanol, 5% Cremophor EL, and 85% D5W [5% (wt/v) dextrose in water]} as previously described (16). Vehicle and SW treatments were performed in six independent experiments for aging studies that included young and aged vehicle- and SW-treated groups. Mice were randomized based on their body weight into vehicle-treated control and SW-treated experimental groups before the start of injections. A full-body necropsy was performed on all mice at the experimental endpoint, and mice that developed tumors were excluded from the study.

Mice undergoing SNT/crush injury—Nerve injury was induced as described below. Mice were treated with SW or vehicle as control intraperitoneally once daily for 14 dpi, starting on the day of the injury, as described above.

SNT surgery

Mice were injected with 1 mg/kg of body weight with buprenorphine SRTM LAB subcutaneously 30 min before the surgery for post-op pain management. Mice were anesthetized with 3% isoflurane. The right leg was shaved from knee to hip and sterilized. A 0.5-cm incision was introduced parallel to the femur approximately 1.5 mm anterior to the femur. Hamstring muscles were located and separated using autoclaved sharp sticks to allow access to the sciatic nerve. The sciatic nerve was firmly held using hemostatic forceps (Fine

Science Tools, 13020–12), and, then, ~5 mm of the nerve was transected using fine sterile scissors. The incision was then closed using 7-mm autoclaved reflex clips (World Precision Instruments, 500344; Applier: 500345). Mice were monitored for recovery from anesthesia and then returned to their home cages.

SNC surgery

The SNC surgery was adopted from the protocol described previously by Bauder and Ferguson (61). The crush surgery was performed as described above with the after modifications. After locating the sciatic nerve, the nerve was mobilized gently with sharp sticks for easy access with hemostatic forceps (Fine Science Tools, 13020–12). Next, the nerve was gently placed on the bottom jaw of the forceps and was crushed for 15 s at three clicks of the forceps (first location of the locking handle). The incision was closed using 7-mm autoclaved reflex clips (World Precision Instruments, 500344; Applier: 500345). Mice were monitored for recovery from anesthesia and then returned to their home cages.

In vivo muscle force measurement

We measured plantar flexion peak tetanic force (millinewton) in mice as described previously (16, 62, 63). Briefly, mice were anesthetized with 3% isoflurane mixed with oxygen, and legs were shaved from ankle to hip to allow for reproducible access to the tibial nerve. The foot was taped to a footplate attached to a servomotor (Aurora Scientific, 300C-LR), and the knee joint was secured to a fixed steel post. Contractions were elicited by percutaneous electrical stimulation of the tibial nerve by inserting two Pt-Ir electrode needles (Aurora Scientific) posterior to the knee joint. The peak isometric torque was achieved by injecting 0.4-mA current to the tibial nerve at a frequency of 150 Hz and a 0.1-ms square wave pulse. We performed three tetanic measurements on each muscle, with 1-min recovery between each measurement, and chose the highest value. Force measurement acquisition was blinded, and the researcher performing the force measurements was unaware of treatment conditions. Data were analyzed using Aurora Scientific Dynamic Muscle Analysis Software Suite. Force was measured longitudinally in mice undergoing unilateral SNC injury on days 3, 7, and 14 after nerve crush. We measured peak tetanic force generated by contralateral uninjured legs in all experimental mice at all time points.

Statistical analysis

Statistical analysis was performed using GraphPad Prism 9 software. A P value of <0.05 was considered significant for all statistical tests. Statistical tests used in each figure panel are described in the corresponding figure legends. A summary of statistical tests and numerical P values for the data presented here is provided in table S1.

Supplementary Material

Refer to Web version on PubMed Central for supplementary material.

Acknowledgments:

We commemorate this paper to D. M. Burns in loving memory of an inspirational colleague. We thank M. Mayerle for editing and proofreading, C. Holbrook and K. Koleckar for technical support, and C. Paulazzo for administrative

support. We thank M. Estrada and S. Howard for the histotechnological support and S. Faulker for the mass spectrometric bioanalytical analysis of muscle tissue sample prostaglandins. We thank the patients whose muscle biopsies were used in the study.

Funding:

This work used the Xevo TQ-XS mass spectrometer system (RRID:SCR_018510) that was purchased with funding from National Institutes of Health Shared Instrumentation grant S10OD026962. M.A.B. was supported by School of Medicine Dean's Postdoctoral Fellowship. Y.X.W. was supported by the Canadian Institutes of Health Research grant MFE-152457, Stanford Translational Research and Applied Medicine (TRAM) Pilot grant, and NIH K99/R00 awards K99NS120278 and R00NS120278. Partial funding for mass spectrometry analysis was provided by the Stanford Dean of Research – SUMS Seed Grant Program. This study was supported by the Donald E. and Delia B. Baxter Foundation; the Li Ka Shing Foundation; Milky Way Research Foundation MWRF-216064; California Institute for Regenerative Medicine grant DISC2-10604; and U.S. National Institutes of Health (NIH) grants R01-AG020961, R01-AG069858, and R01-RHG009674 to H.M.B.

Data and materials availability:

All data associated with this study are present in the paper or the Supplementary Materials. Sequencing data have been uploaded to GEO (data series GSE239848). Experimental data and any additional information required to reanalyze the data reported here are available upon request. Correspondence should be addressed to H.M.B and Y.X.W.

REFERENCES AND NOTES

1. Dieleman JL, Cao J, Chapin A, Chen C, Li Z, Liu A, Horst C, Kaldjian A, Matyasz T, Scott KW, Bui AL, Campbell M, Duber HC, Dunn AC, Flaxman AD, Fitzmaurice C, Naghavi M, Sadat N, Shieh P, Squires E, Yeung K, Murray CJL, US health care spending by payer and health condition, 1996–2016. JAMA 323, 863–884 (2020). [PubMed: 32125402]
2. Beaudart C, Rizzoli R, Bruyère O, Reginster J-Y, Biver E, Sarcopenia: Burden and challenges for public health. Arch. Public Health 72, 45 (2014). [PubMed: 25810912]
3. Li L, Xiong W-C, Mei L, Neuromuscular junction formation, aging, and disorders. Annu. Rev. Physiol. 80, 159–188 (2018). [PubMed: 29195055]
4. Fralish Z, Lotz EM, Chavez T, Khodabukus A, Bursac N, Neuromuscular development and disease: Learning from in vitro and in vivo models. Front. Cell Dev. Biol. 9, 764732 (2021). [PubMed: 34778273]
5. Burden SJ, Yumoto N, Zhang W, The role of MuSK in synapse formation and neuromuscular disease. Cold Spring Harb. Perspect. Biol. 5, a009167 (2013). [PubMed: 23637281]
6. DeChiara TM, Bowen DC, Valenzuela DM, Simmons MV, Poueymirou WT, Thomas S, Kinetz E, Compton DL, Rojas E, Park JS, Smith C, DiStefano PS, Glass DJ, Burden SJ, Yancopoulos GD, The receptor tyrosine kinase MuSK is required for neuromuscular junction formation in vivo. Cell 85, 501–512 (1996). [PubMed: 8653786]
7. Kim N, Burden SJ, MuSK controls where motor axons grow and form synapses. Nat. Neurosci. 11, 19–27 (2008). [PubMed: 18084289]
8. Kim N, Stiegler AL, Cameron TO, Hallock PT, Gomez AM, Huang JH, Hubbard SR, Dustin ML, Burden SJ, Lrp4 is a receptor for Agrin and forms a complex with MuSK. Cell 135, 334–342 (2008). [PubMed: 18848351]
9. Ahn Jo S, Zhu X, Marchionni MA, Burden SJ, Neuregulins are concentrated at nerve-muscle synapses and activate ACh–receptor gene expression. Nature 373, 158–161 (1995). [PubMed: 7816098]
10. Valdez G, Tapia JC, Kang H, Clemenson GD, Gage FH, Lichtman JW, Sanes JR, Attenuation of age-related changes in mouse neuromuscular synapses by caloric restriction and exercise. Proc. Natl. Acad. Sci. U.S.A. 107, 14863–14868 (2010). [PubMed: 20679195]
11. Liu W, Klose A, Forman S, Paris ND, Wei-LaPierre L, Cortés-Lopéz M, Tan A, Flaherty M, Miura P, Dirksen RT, Chakkalakal JV, Loss of adult skeletal muscle stem cells drives age-related neuromuscular junction degeneration. eLife 6, e26464 (2017). [PubMed: 28583253]

12. Soendenbroe C, Andersen JL, Mackey AL, Muscle-nerve communication and the molecular assessment of human skeletal muscle denervation with aging. Am. J. Physiol. Cell Physiol. 321, C317–C329 (2021). [PubMed: 34161153]
13. Carnio S, LoVerso F, Baraibar MA, Longa E, Khan MM, Maffei M, Reischl M, Canepari M, Loefler S, Kern H, Blaauw B, Friguet B, Bottinelli R, Rudolf R, Sandri M, Autophagy impairment in muscle induces neuromuscular junction degeneration and precocious aging. Cell Rep. 8, 1509–1521 (2014). [PubMed: 25176656]
14. Arnold A-S, Gill J, Christe M, Ruiz R, McGuirk S, St-Pierre J, Tabares L, Handschin C, Morphological and functional remodelling of the neuromuscular junction by skeletal muscle PGC-1α. Nat. Commun. 5, 3569 (2014). [PubMed: 24686533]
15. Ho ATV, Palla AR, Blake MR, Yucel ND, Wang YX, Magnusson KEG, Holbrook CA, Kraft PE, Delp SL, Blau HM, Prostaglandin E2 is essential for efficacious skeletal muscle stem-cell function, augmenting regeneration and strength. Proc. Natl. Acad. Sci. U.S.A. 114, 6675–6684 (2017). [PubMed: 28607093]
16. Palla AR, Ravichandran M, Wang YX, Alexandrova L, Yang AV, Kraft P, Holbrook CA, Schürch CM, Ho ATV, Blau HM, Inhibition of prostaglandin-degrading enzyme 15-PGDH rejuvenates aged muscle mass and strength. Science 371, eabc8059 (2021). [PubMed: 33303683]
17. Engel WK, Muscle target fibres, a newly recognized sign of denervation. Nature 191, 389–390 (1961). [PubMed: 13696814]
18. Schürch CM, Bhate SS, Barlow GL, Phillips DJ, Noti L, Zlobec I, Chu P, Black S, Demeter J, McIlwain DR, Kinoshita S, Samusik N, Goltsev Y, Nolan GP, Coordinated cellular neighborhoods orchestrate antitumoral immunity at the colorectal cancer invasive front. Cell 182, 1341–1359.e19 (2020). [PubMed: 32763154]
19. Wang YX, Holbrook CA, Hamilton JN, Garoussian J, Afshar M, Su S, Schürch CM, Lee MY, Goltsev Y, Kundaje A, Nolan GP, Blau HM, A single cell spatial temporal atlas of skeletal muscle reveals cellular neighborhoods that orchestrate regeneration and become disrupted in aging (2022). 10.1101/2022.06.10.494732.
20. Ehmsen JT, Kawaguchi R, Mi R, Coppola G, Höke A, Longitudinal RNA-Seq analysis of acute and chronic neurogenic skeletal muscle atrophy. Sci. Data 6, 179 (2019). [PubMed: 31551418]
21. McCormack NM, Villalón E, Viollet C, Soltis AR, Dalgard CL, Lorson CL, Burnett BG, Survival motor neuron deficiency slows myoblast fusion through reduced myomaker and myomixer expression. J. Cachexia. Sarcopenia Muscle 12, 1098–1116 (2021). [PubMed: 34115448]
22. Wang D, Dubois RN, Eicosanoids and cancer. Nat. Rev. Cancer 10, 181–193 (2010). [PubMed: 20168319]
23. Wu Y-H, Ko T-P, Guo R-T, Hu S-M, Chuang L-M, Wang AH-J, Structural basis for catalytic and inhibitory mechanisms of human prostaglandin reductase PTGR2. Structure 16, 1714–1723 (2008). [PubMed: 19000823]
24. Frey D, Schneider C, Xu L, Borg J, Spooren W, Caroni P, Early and selective loss of neuromuscular synapse subtypes with low sprouting competence in motoneuron diseases. J. Neurosci. 20, 2534–2542 (2000). [PubMed: 10729333]
25. Einsiedel LJ, Luff AR, Alterations in the contractile properties of motor units within the ageing rat medial gastrocnemius. J. Neurol. Sci. 112, 170–177 (1992). [PubMed: 1469429]
26. Lexell J, Human aging, muscle mass, and fiber type composition. J. Gerontol. A Biol. Sci. Med. Sci. 50 Spec No, 11–16 (1995). [PubMed: 7493202]
27. Chai RJ, Vukovic J, Dunlop S, Grounds MD, Shavlakadze T, Striking denervation of neuromuscular junctions without lumbar motoneuron loss in geriatric mouse muscle. PLOS ONE 6, e28090 (2011). [PubMed: 22164231]
28. Pun S, Santos AF, Saxena S, Xu L, Caroni P, Selective vulnerability and pruning of phasic motoneuron axons in motoneuron disease alleviated by CNTF. Nat. Neurosci. 9, 408–419 (2006). [PubMed: 16474388]
29. Petrany MJ, Swoboda CO, Sun C, Chetal K, Chen X, Weirauch MT, Salomonis N, Millay DP, Single-nucleus RNA-seq identifies transcriptional heterogeneity in multinucleated skeletal myofibers. Nat. Commun. 11, 6374 (2020). [PubMed: 33311464]

30. Dos Santos M, Backer S, Saintpierre B, Izac B, Andrieu M, Letourneur F, Relaix F, Sotiropoulos A, Maire P, Single-nucleus RNA-seq and FISH identify coordinated transcriptional activity in mammalian myofibers. Nat. Commun. 11, 5102 (2020). [PubMed: 33037211]
31. Ehmsen JT, Kawaguchi R, Kaval D, Johnson AE, Nachun D, Coppola G, Höke A, GADD45A is a protective modifier of neurogenic skeletal muscle atrophy. JCI Insight 6, e149381 (2021). [PubMed: 34128833]
32. Memme JM, Oliveira AN, Hood DA, p53 regulates skeletal muscle mitophagy and mitochondrial quality control following denervation-induced muscle disuse. J. Biol. Chem. 298, 101540 (2022). [PubMed: 34958797]
33. Luo L, Martin SC, Parkington J, Cadena SM, Zhu J, Ibebunjo C, Summermatter S, Londraville N, Patora-Komisarska K, Widler L, Zhai H, Trendelenburg A-U, Glass DJ, Shi J, HDAC4 controls muscle homeostasis through deacetylation of myosin heavy chain, PGC-1α, and Hsc70. Cell Rep. 29, 749–763.e12 (2019). [PubMed: 31618641]
34. Moresi V, Williams AH, Meadows E, Flynn JM, Potthoff MJ, McAnally J, Shelton JM, Backs J, Klein WH, Richardson JA, Bassel-Duby R, Olson EN, Myogenin and class II HDACs control neurogenic muscle atrophy by inducing E3 ubiquitin ligases. Cell 143, 35–45 (2010). [PubMed: 20887891]
35. Yagishita S, Itoh Y, Target-targetoid phenomenon of the human muscle fibers. A histological, histochemical and ultrastructural study. Virchows Arch. A Pathol. Anat. Histol. 375, 13–22 (1977). [PubMed: 143767]
36. Joyce NC, Oskarsson B, Jin L-W, Muscle biopsy evaluation in neuromuscular disorders. Phys. Med. Rehabil. Clin. N. Am. 23, 609–631 (2012). [PubMed: 22938878]
37. Dubowitz V, Pathology of experimentally re-innervated skeletal muscle. J. Neurol. Neurosurg. Psychiatry 30, 99–110 (1967). [PubMed: 4226750]
38. Dubowitz V, Sewry CA, PhD MD AO, Muscle Biopsy: A Practical Approach: Expert Consult; Online and Print (Elsevier Health Sciences, 2013).
39. Berry JA, Elia C, Saini HS, Miulli DE, A review of lumbar radiculopathy, diagnosis, and treatment. Cureus 11, e5934 (2019). [PubMed: 31788391]
40. Sanes JR, Marshall LM, McMahan UJ, Reinnervation of muscle fiber basal lamina after removal of myofibers. Differentiation of regenerating axons at original synaptic sites. J. Cell Biol. 78, 176–198 (1978). [PubMed: 307554]
41. Magill CK, Tong A, Kawamura D, Hayashi A, Hunter DA, Parsadanian A, Mackinnon SE, Myckatyn TM, Reinnervation of the tibialis anterior following sciatic nerve crush injury: A confocal microscopic study in transgenic mice. Exp. Neurol. 207, 64–74 (2007). [PubMed: 17628540]
42. Bermedo-García F, Zelada D, Martínez E, Tabares L, Henríquez JP, Functional regeneration of the murine neuromuscular synapse relies on long-lasting morphological adaptations. BMC Biol. 20, 158 (2022). [PubMed: 35804361]
43. Dalkin W, Taetzsch T, Valdez G, The fibular nerve injury method: A reliable assay to identify and test factors that repair neuromuscular junctions. J. Vis. Exp. 114, 54186 (2016).
44. Nango H, Kosuge Y, Miyagishi H, Sugawa K, Ito Y, Ishige K, Prostaglandin E2 facilitates neurite outgrowth in a motor neuron-like cell line, NSC-34. J. Pharmacol. Sci. 135, 64–71 (2017). [PubMed: 28966102]
45. Gao Y, Deng K, Hou J, Bryson JB, Barco A, Nikulina E, Spencer T, Mellado W, Kandel ER, Filbin MT, Activated CREB Is sufficient to overcome inhibitors in myelin and promote spinal axon regeneration in vivo. Neuron 44, 609–621 (2004). [PubMed: 15541310]
46. Hannila SS, Filbin MT, The role of cyclic AMP signaling in promoting axonal regeneration after spinal cord injury. Exp. Neurol. 209, 321–332 (2008). [PubMed: 17720160]
47. Blum JA, Klemm S, Shadrach JL, Guttenplan KA, Nakayama L, Kathiria A, Hoang PT, Gautier O, Kaltschmidt JA, Greenleaf WJ, Gitler AD, Single-cell transcriptomic analysis of the adult mouse spinal cord reveals molecular diversity of autonomic and skeletal motor neurons. Nat. Neurosci. 24, 572–583 (2021). [PubMed: 33589834]
48. Ohno H, Morikawa Y, Hirata F, Studies on 15-hydroxyprostaglandin dehydrogenase with various prostaglandin analogues. J. Biochem. 84, 1485–1494 (1978). [PubMed: 216666]

49. Rowan SL, Rygiel K, Purves-Smith FM, Solbak NM, Turnbull DM, Hepple RT, Denervation causes fiber atrophy and myosin heavy chain co-expression in senescent skeletal muscle. PLOS ONE 7, e29082 (2012). [PubMed: 22235261]
50. Liang X, Lin L, Woodling NS, Wang Q, Anacker C, Pan T, Merchant M, Andreasson K, Signaling via the prostaglandin E_2 receptor EP4 exerts neuronal and vascular protection in a mouse model of cerebral ischemia. J. Clin. Invest. 121, 4362–4371 (2011). [PubMed: 21965326]
51. Li M, Ona VO, Guégan C, Chen M, Jackson-Lewis V, Andrews LJ, Olszewski AJ, Stieg PE, Lee JP, Przedborski S, Friedlander RM, Functional role of caspase-1 and caspase-3 in an ALS transgenic mouse model. Science 288, 335–339 (2000). [PubMed: 10764647]
52. Pasinelli P, Houseweart MK, Brown RH, Cleveland DW, Caspase-1 and -3 are sequentially activated in motor neuron death in Cu,Zn superoxide dismutase-mediated familial amyotrophic lateral sclerosis. Proc. Natl. Acad. Sci. U.S.A. 97, 13901–13906 (2000). [PubMed: 11095709]
53. Guégan C, Vila M, Rosoklija G, Hays AP, Przedborski S, Recruitment of the mitochondrial-dependent apoptotic pathway in amyotrophic lateral sclerosis. J. Neurosci. 21, 6569–6576 (2001). [PubMed: 11517246]
54. Huebner EA, Strittmatter SM, Axon regeneration in the peripheral and central nervous systems. Results Probl. Cell Differ. 48, 339–351 (2009). [PubMed: 19582408]
55. Stoll G, Griffin JW, Li CY, Trapp BD, Wallerian degeneration in the peripheral nervous system: Participation of both Schwann cells and macrophages in myelin degradation. J. Neurocytol. 18, 671–683 (1989). [PubMed: 2614485]
56. Vargas ME, Barres BA, Why Is Wallerian degeneration in the CNS so slow? Annu. Rev. Neurosci. 30, 153–179 (2007). [PubMed: 17506644]
57. Handschin C, Kobayashi YM, Chin S, Seale P, Campbell KP, Spiegelman BM, PGC-1α regulates the neuromuscular junction program and ameliorates Duchenne muscular dystrophy. Genes Dev. 21, 770–783 (2007). [PubMed: 17403779]
58. Khan MM, Strack S, Wild F, Hanashima A, Gasch A, Brohm K, Reischl M, Carnio S, Labeit D, Sandri M, Labeit S, Rudolf R, Role of autophagy, SQSTM1, SH3GLB1, and TRIM63 in the turnover of nicotinic acetylcholine receptors. Autophagy 10, 123–136 (2014). [PubMed: 24220501]
59. Rudolf R, Bogomolovas J, Strack S, Choi K-R, Khan MM, Wagner A, Brohm K, Hanashima A, Gasch A, Labeit D, Labeit S, Regulation of nicotinic acetylcholine receptor turnover by MuRF1 connects muscle activity to endo/lysosomal and atrophy pathways. Age 35, 1663–1674 (2013). [PubMed: 22956146]
60. Oury J, Zhang W, Leloup N, Koide A, Corrado AD, Ketavarapu G, Hattori T, Koide S, Burden SJ, Mechanism of disease and therapeutic rescue of *Dok7* congenital myasthenia. Nature 595, 404–408 (2021). [PubMed: 34163073]
61. Bauder AR, Ferguson TA, Reproducible mouse sciatic nerve crush and subsequent assessment of regeneration by whole mount muscle analysis. J. Vis. Exp. 60, e3606 (2012).
62. Sheth KA, Iyer CC, Wier CG, Crum AE, Bratasz A, Kolb SJ, Clark BC, Burghes AHM, Arnold WD, Muscle strength and size are associated with motor unit connectivity in aged mice. Neurobiol. Aging 67, 128–136 (2018). [PubMed: 29656012]
63. Mintz EL, Passipieri JA, Lovell DY, Christ GJ, Applications of in vivo functional testing of the rat tibialis anterior for evaluating tissue engineered skeletal muscle repair. J. Vis. Exp. 116, 54487 (2016).
64. Richner M, Jager SB, Siupka P, Vaegter CB, Hydraulic extrusion of the spinal cord and isolation of dorsal root ganglia in rodents. J. Vis. Exp. 119, 55226 (2017).
65. Biodock, Biodock, AI Software Platform (2023); www.biodock.ai/.
66. Prasain JK, Hoang HD, Edmonds JW, Miller MA, Prostaglandin extraction and analysis in Caenorhabditis elegans. J. Vis. Exp. 76, 50447 (2013).

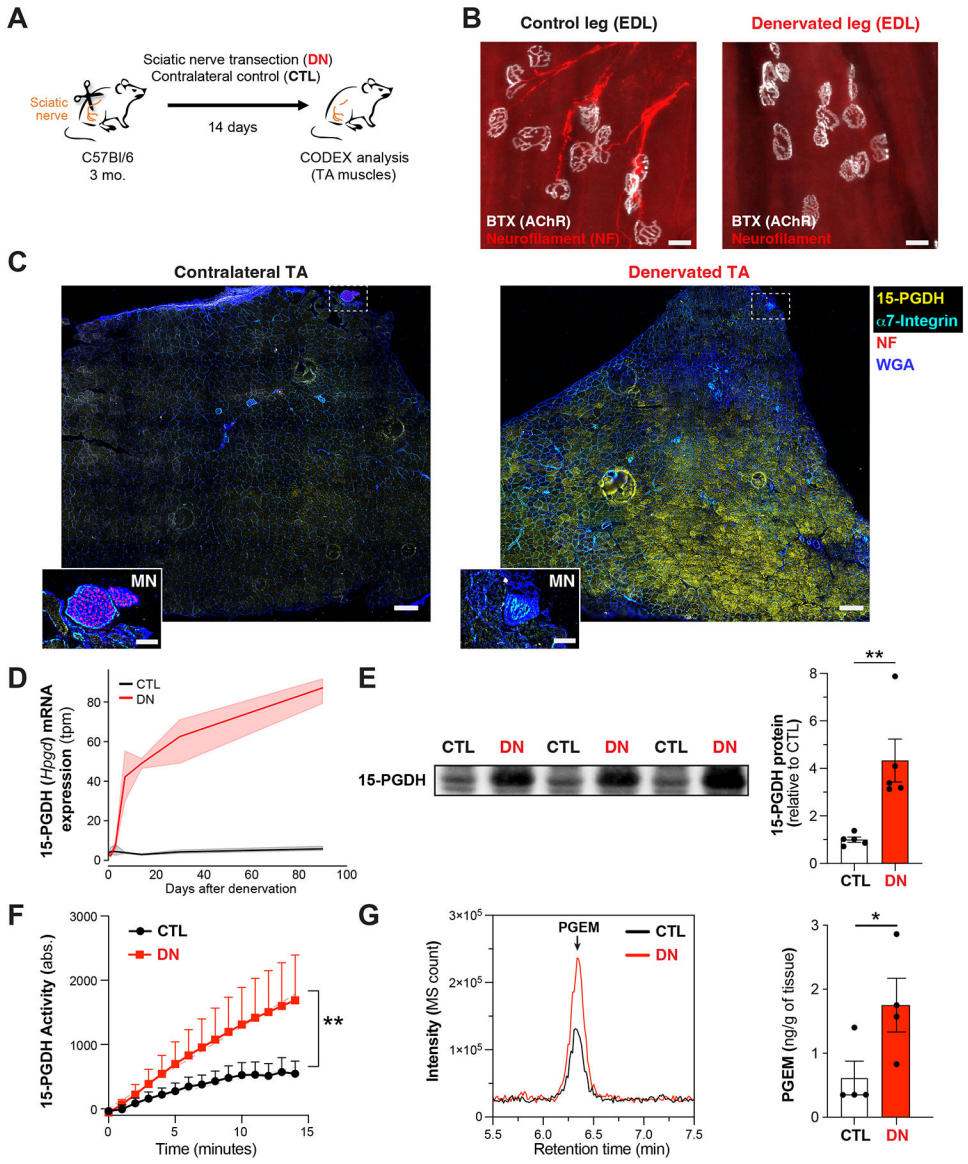

Fig. 1. 15-PGDH expression is induced by muscle denervation in mice.

(**A**) Experimental scheme of unilateral sciatic nerve transection (SNT) leading to denervation analyzed 14 dpi. (**B**) Representative images of whole-mount EDL muscles immunostained for NF (red) and BTX (gray) to visualize AChRs in control (left) and denervated (right) legs at 14 dpi. Scale bars, 20 μm. (**C**) Representative CODEX immunofluorescence images of control (left) and denervated (right) TA muscle transverse sections 14 dpi to codetect 15-PGDH (yellow), cell membrane [wheat germ agglutinin (WGA); blue), NF (inset; red), and α7 integrin (inset; cyan). Insets are magnified regions of white dashed rectangles in (C) highlighting TA nerve tracts. Insets are ×3.6 magnified compared with the main panels. Scale bars, 100 μm; inset scale bars, 25 μm. (**D**) Time course of normalized mRNA expression data (20) analyzed for 15-PGDH (*Hpgd*) expression in denervated (DN; red) and contralateral control (CTL; black) GA muscles. Translucent error bands show the SEM. (**E**) Left: Representative Western blot images of 15-PGDH in

control and denervated GA muscles of mice 14 dpi. Right: Quantification of 15-PGDH Western blots normalized to total protein ($n = 5$ mice, data are represented as means ± SEM). Unpaired *t* test. (**F**) Kinetic measurement of 15-PGDH enzymatic activity in GA muscle lysates from four mice control (black) and denervated (red) legs 14 dpi. Unpaired *t* test. (**G**) Left: Representative chromatogram of PGE2 breakdown product PGEM peak intensities expressed as MS counts in contralateral control (black) and denervated (red) GA muscles analyzed by LC-MS/MS at 14 dpi. Right: Quantification of PGEM in GA muscles quantified by LC-MS/MS ($n = 4$ mice, data are represented as means ± SEM) at 14 dpi. Paired *t* test. $^{*}P < 0.05$ and $^{**}P < 0.01$. MN, motor neurons.

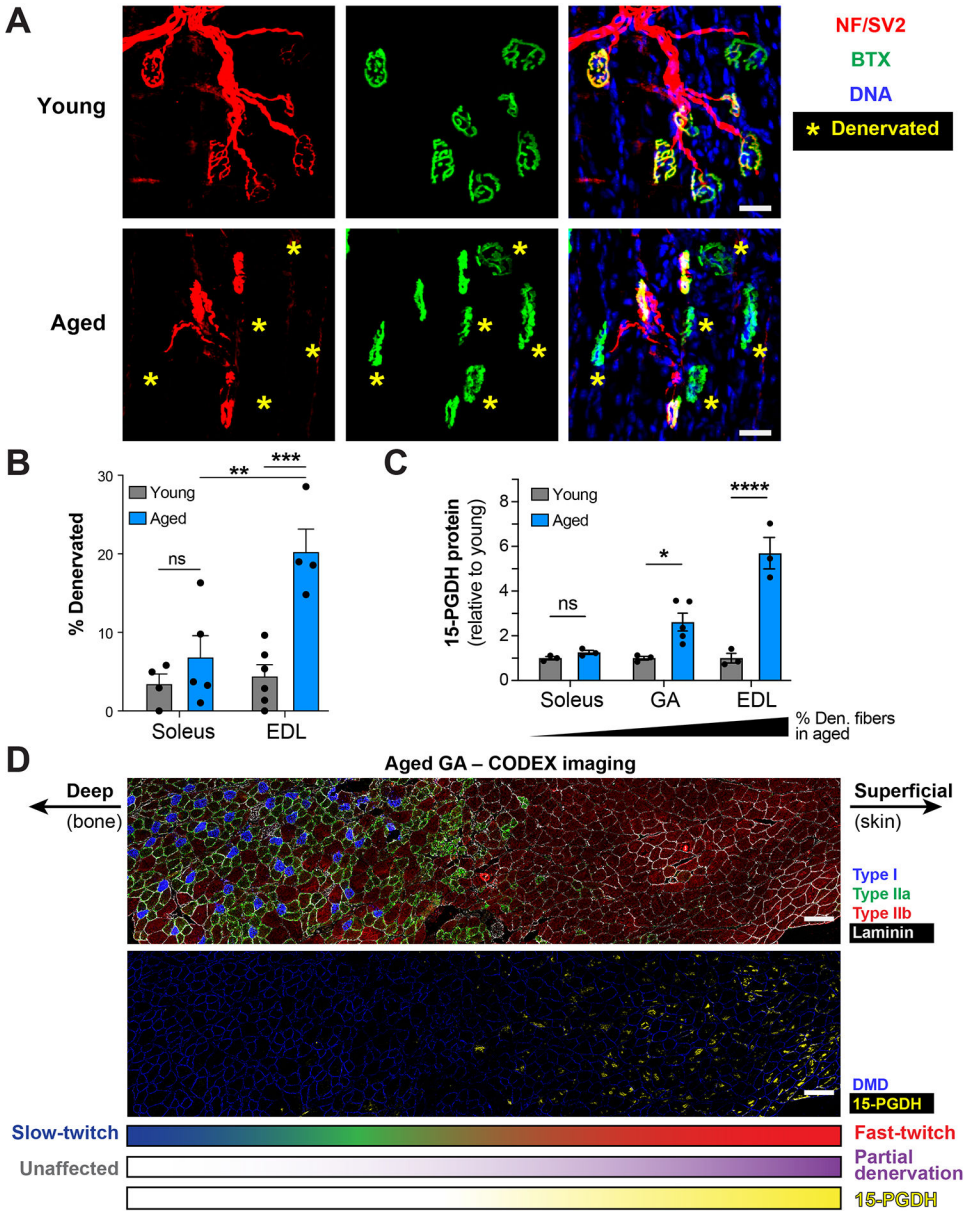

Fig. 2. Denervated myofibers in aged mice exhibit increased 15-PGDH expression.

(**A**) Representative confocal images of NMJs in EDL muscles of young (top) and aged (bottom) mice. Whole-mount muscle tissues were immunostained to visualized presynaptic motor neurons (NF + SV2; red). Postsynaptic AChRs are visualized with fluorophore-conjugated BTX (green). Nuclei are stained with Hoechst. NMJs labeled with an asterisk are denervated [devoid of presynaptic (red) signal]. Scale bars, 40 μm. (**B**) Quantification of denervated myofibers (% total) in young (gray bars) and aged (blue bars) Sol and EDL muscles. (Sol: $n = 4$ young and $n = 5$ aged mice; EDL: $n = 6$ young and $n = 4$ aged mice). Two-way analysis of variance (ANOVA). (**C**) Quantification of 15-PGDH relative to total protein in young (gray bars) and aged (blue bars) soleus (slow-twitch), GA (mixed fiber type), and EDL (fast-twitch) muscles (Sol, $n = 3$ young and $n = 3$ aged mice; GA, $n = 3$ young and $n = 5$ aged mice; EDL, $n = 3$ young and $n = 3$ aged mice). Two-way ANOVA. (**D**)

Top: Representative CODEX image of aged lateral GA muscle immunostained to visualize myofiber subtypes (type I, blue; type IIa, green; and type IIb, red) and muscle basal lamina (laminin; gray). Bottom: Representative CODEX image of the same region shown in the top panel immunostained to visualize 15-PGDH (yellow) and dystrophin (DMD; blue). Scale bars, 100 μm. Data in (B) and (C) are presented as means ± SEM. *$P < 0.05$, **$P < 0.01$, ***$P < 0.001$, and ****$P < 0.0001$. ns, not significant.

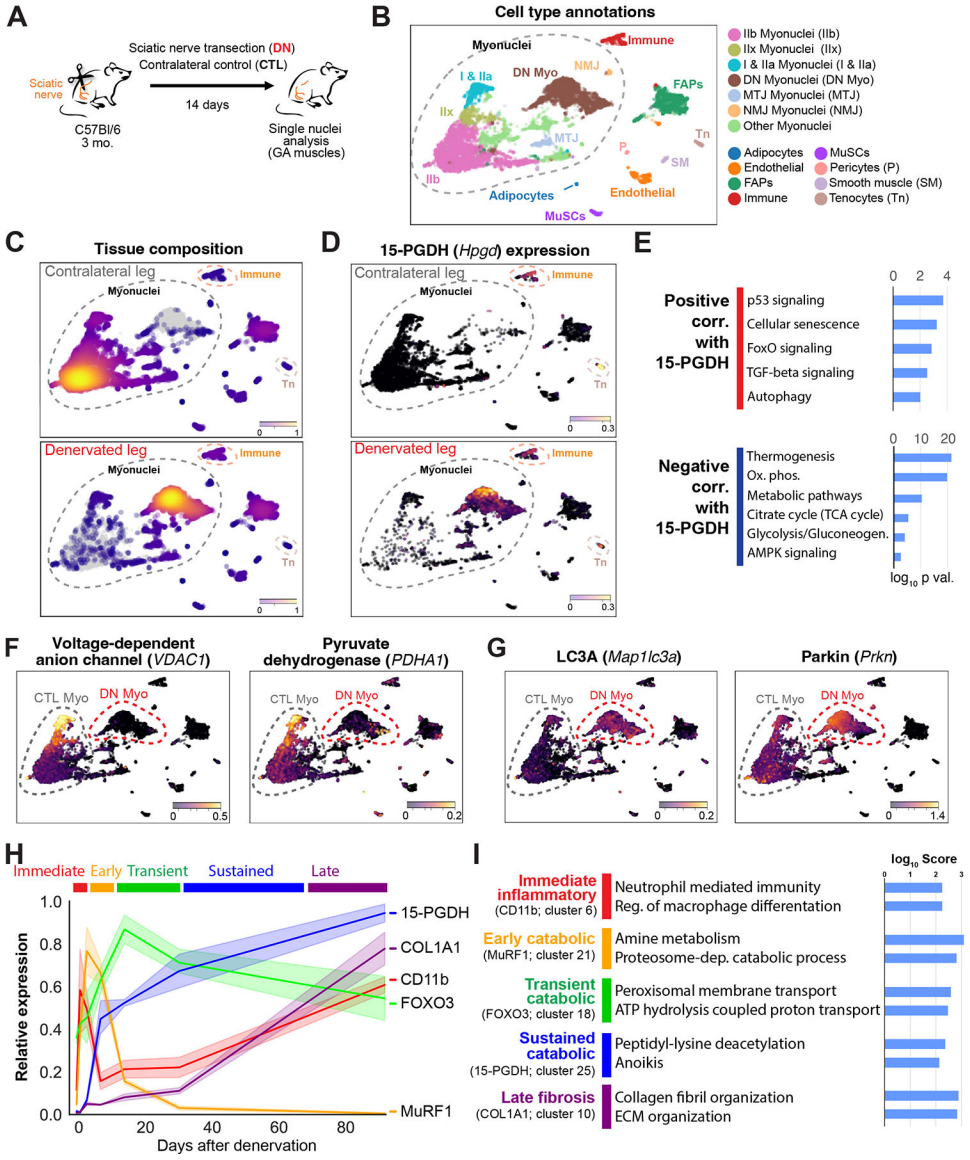

Fig. 3. 15-PGDH is part of a distinct sustained gene expression program triggered by denervation.

(**A**) Experimental scheme for single nuclei acquired from contralateral control and denervated GA muscles of mice after SNT at 14 days postinjury (dpi). (**B**) Annotations of cell types identified in a single-nucleus analysis of denervated GA muscles plotted in an uniform manifold approximation and projection (UMAP) embedding. Each color denotes a cell type identified by clustering on the basis of gene expression. (**C**) Kernel density estimation of the cell-type composition for nuclei found in the contralateral leg (top) versus the denervated leg (bottom). (**D**) Expression of 15-PGDH (*Hpgd*) detected in each nucleus. (**E**) Gene ontology (GO) terms enriched for genes that positively correlate [correlation coefficient (r) > 0.5; top set] or negatively correlate ($r < -0.3$; bottom set) with 15-PGDH (*Hpgd*) expression in myonuclei. AMPK, 5’ adenosine monophosphate-activated protein kinase; TCA, tricarboxylic acid cycle. (**F**) Expression of mitochondrial membrane *Vdac1* (top) and mitochondrial enzyme *Pdha1* (bottom) detected in each nucleus acquired

from control and denervated muscles of mice after SNT at 14 dpi. (**G**) Expression of autophagy marker *Map1lc3a* and the mitophagy marker *Prkn* detected in each nucleus acquired from control and denervated muscles of mice after SNT at 14 dpi. (**H**) Time course of mRNA expression (normalized to minimum and maximum expression for each gene over the time course) patterns of denervation-associated genes CD11b (*Itgam*; red), muscle RING-finger protein-1 (MuRF1) (*Trim63*; orange), *FoxO3* (green), 15-PGDH (*Hpgd*; blue), and *COL1A1* (purple). Translucent error bands show the SEM for each gene. (**I**) GO terms enriched for each temporally distinct gene set (cluster) of denervation genes highlighted in (A). Coregulated gene sets correspond to immediate inflammatory markers that enrich in neutrophil and macrophage infiltration GO terms (red); early and transient catabolic genes include the atrogene MuRF1 (*Trim63*), other proteosome-associated atrogenes, and the downstream mediator of protein degradation forkhead box protein O3 (FOXO3; orange and green); sustained genes including 15-PGDH and HDAC4 that enrich in protein deacetylation and anoikis GO terms (blue); and late genes that enrich in fibrotic ECM GO terms (purple). Gene set clusters and GO terms are found in fig. S4A and data file S1. In (D) to (G), each dot denotes a nucleus. Tn, tenocytes; FAP, fibroadipogenic progenitors.

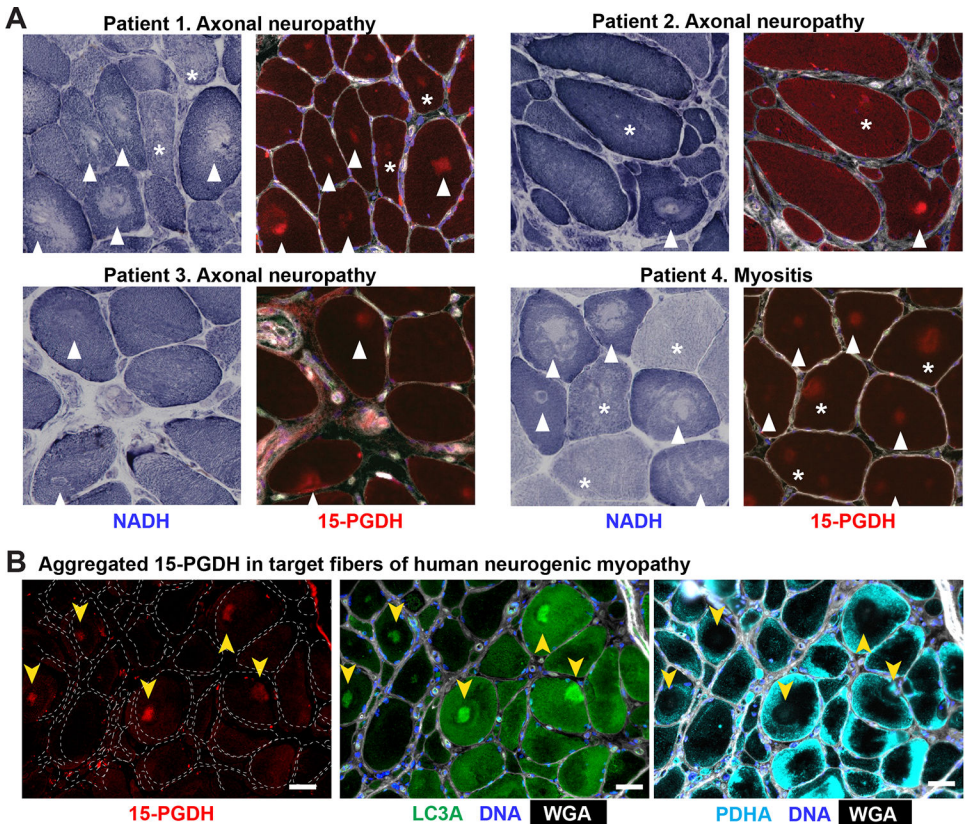

Fig. 4. 15-PGDH aggregation is a marker of human neurogenic myopathies.

(**A**) Representative images of muscle biopsies from patients with neurogenic myopathies resulting from axonal neuropathies and myositis. Serial sections were used to match NADH–tetrazolium reductase staining (left panels) and immunostaining for 15-PGDH (red; right panels). White arrowheads indicate target fibers with central regions lacking NADH staining. Asterisks (*) indicate fibers with 15-PGDH aggregation but apparently normal NADH staining. (**B**) Representative images of muscle biopsy serial sections from a patient diagnosed with neurogenic myopathy resulting from amyloidosis immunostained to visualize 15-PGDH (left; red), LC3A (middle; green), cell membrane with WGA (middle and right panels; gray), mitochondrial enzyme PDHA (right; cyan), and cell nuclei [4′,6-diamidino-2-phenylindole (DAPI); blue]. Yellow arrowheads indicate target fibers with central aggregation of 15-PGDH and LC3A. Scale bars, 50 μm.

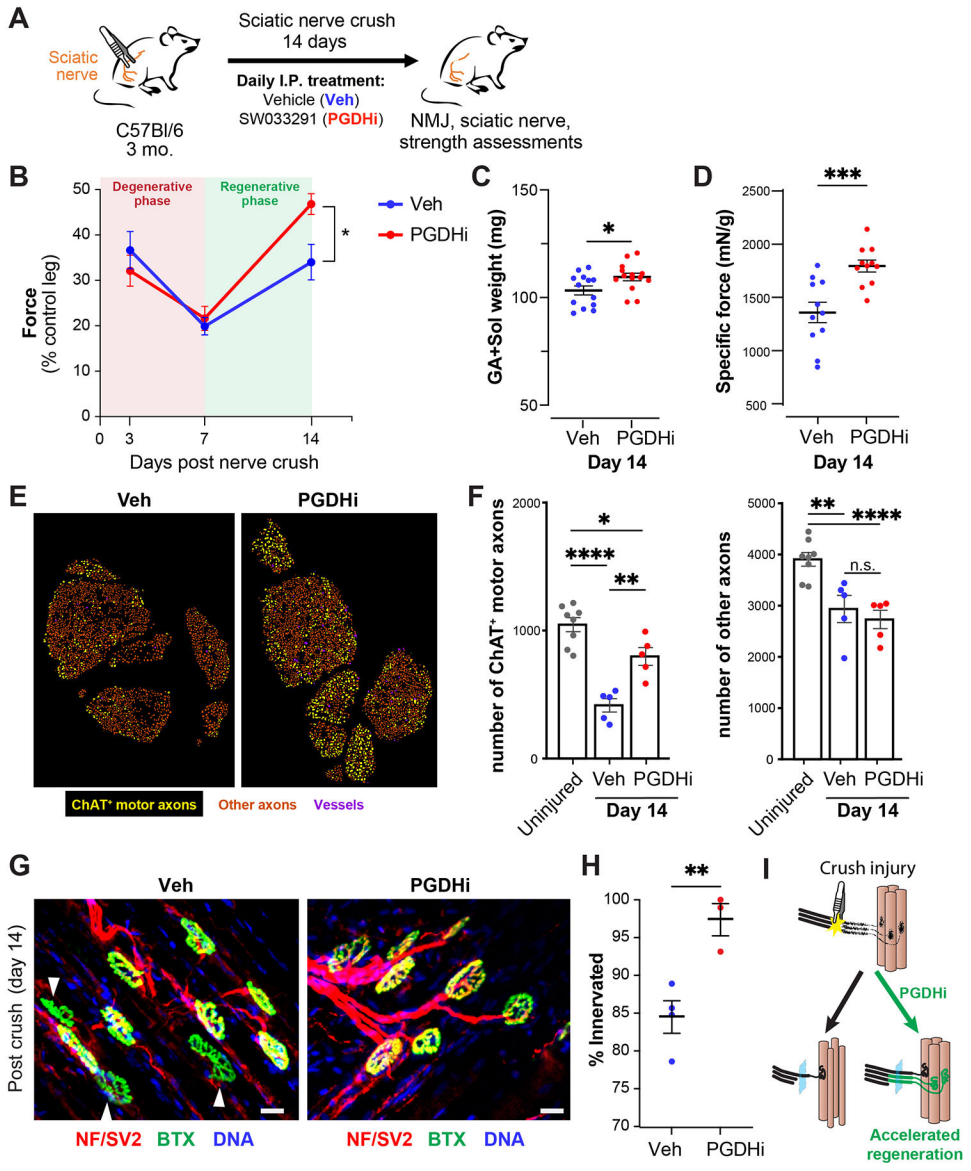

Fig. 5. PGDHi accelerates recovery from nerve crush injury in mice.

(**A**) Experimental scheme. Mice were injected daily intraperitoneally with PGDHi or vehicle (Veh) after SNC and analyzed 14 dpi. I.P., intraperitoneal. (**B**) Plantar flexion tetanic force (percent of contralateral control leg) measured by electrical stimulation of tibial nerve on days 3, 7, and 14 after SNC injury in vehicle (blue) and PGDHi-treated (red) mice (n = 13 vehicle-treated and n = 14 PGDHi-treated). Two-way ANOVA with Tukey's multiple comparisons test. (**C**) GA and Sol muscle weight for vehicle- (blue) and PGDHi-treated (red) mice 14 dpi (n = 13 vehicle-treated and n = 14 PGDHi-treated). Unpaired t test. (**D**) Muscle specific force (plantar flexion tetanic force normalized to muscle weight) in vehicle- (blue) and PGDHi-treated (red) mice 14 dpi. Unpaired t test. (**E**) Representative pseudo-colored masks of ChAT$^+$ motor axons (yellow), other axons (orange), and blood vessels (purple) in transverse sections of sciatic nerves of vehicle- (left) and PGDHi-treated (right) mice 14 dpi. (**F**) Quantification of ChAT$^+$ motor axons and other axons in transverse

sections of sciatic nerves of healthy (gray; $n = 8$) or vehicle- (blue; $n = 5$) or PGDHi-treated (red; $n = 5$) mice 14 dpi. Two-way ANOVA with Tukey's multiple comparisons test. (**G**) Representative confocal images of NMJs in whole mounts of the EDL muscles of injured legs of mice undergoing unilateral SNC injury 14 dpi. Whole-mount tissues were immunostained with a cocktail of antibodies to presynaptic motor neuronal markers (NF and SV2; red) and fluorophore-conjugated α-BTX (green) to visualize postsynaptic AChRs. Nuclei are stained with Hoechst (blue). Arrowheads (white) indicate denervated NMJs lacking presynaptic (red) signal. Scale bars, 20 μm. (**H**) Quantification of percent denervated myofibers in injured EDLs of mice after SNC 14 dpi treated with either vehicle (blue) or PGDHi (red) at 14 dpi ($n = 4$ vehicle-treated and $n = 3$ PGDHi-treated). Unpaired t test. (**I**) Summary for the mechanism of reinnervation after sciatic nerve injury and PGDHi treatment. *$P < 0.05$, **$P < 0.01$, ***$P < 0.001$, and ****$P < 0.0001$; data in (C) to (F) are presented as means ± SEM.

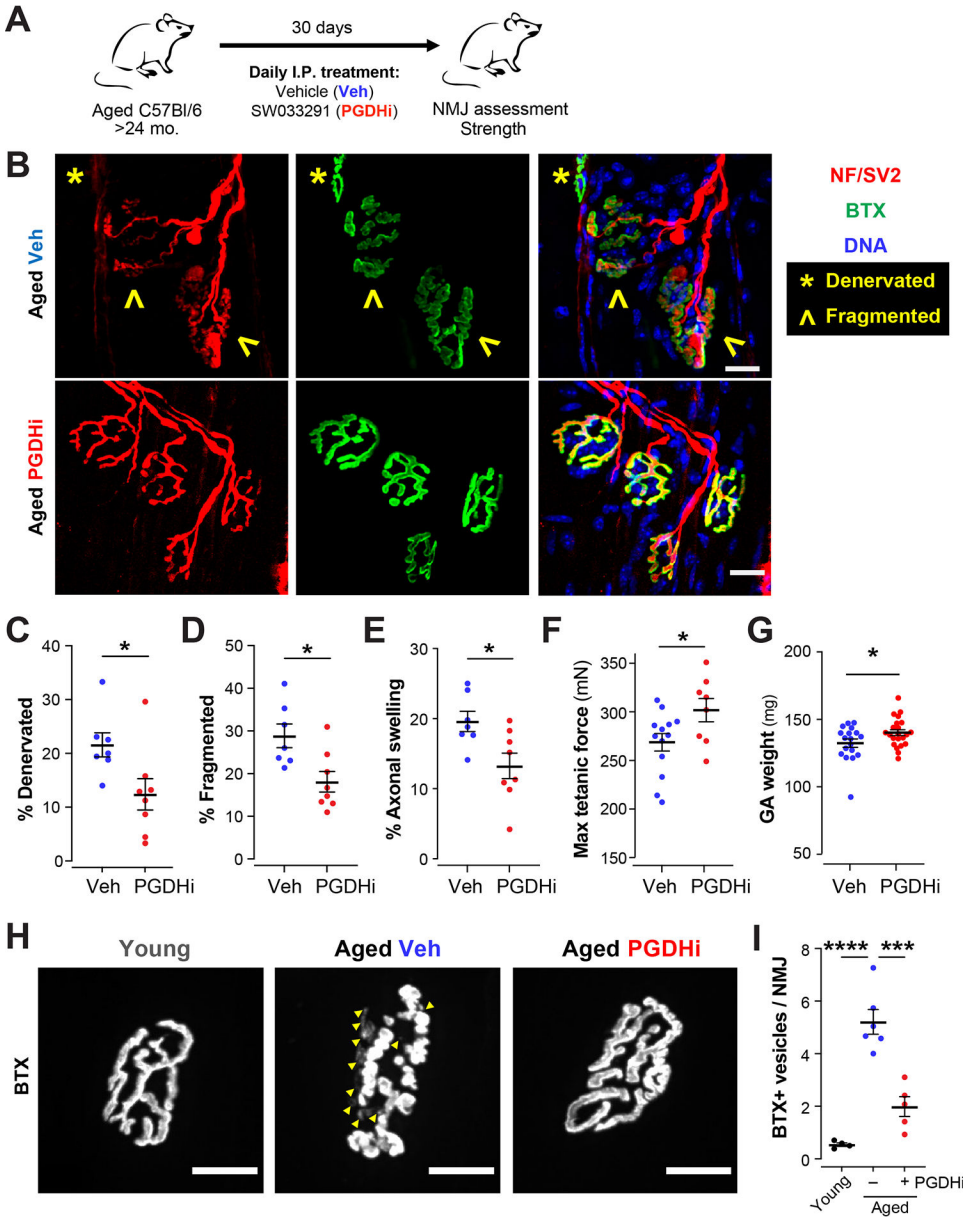

Fig. 6. PGDHi leads to reinnervation of NMJs and increased strength in aged mice.

(**A**) Experimental scheme. Mice were injected daily intraperitoneally with PGDHi or vehicle for 30 days. (**B**) Representative confocal images of NMJs in EDL muscles of aged mice treated with vehicle (top panels) or PGDHi (bottom panels). Whole-mount muscle tissues were immunostained to visualize presynaptic motor neurons (NF + SV2; red). Postsynaptic AChRs are visualized with fluorophore-conjugated BTX (green). Yellow arrowheads indicate morphologically fragmented NMJs, and asterisks (*) indicate denervated NMJs that lack NF + SV2 staining. Nuclei are stained with Hoechst. Scale bars, 20 μm. (**C** to **E**) Quantification of age-related abnormalities [(C) denervation, (D) fragmentation, and (E) axonal swelling] in NMJs from EDL muscles of vehicle-treated (blue; $n = 7$ mice) and PGDHi-treated (red; $n = 8$ mice) aged mice (25 to 27 months). (**F**) Quantification of plantar flexion tetanic force in aged mice treated for 1 month with vehicle (blue) and PGDHi (red)

(**G**) Quantification of GA muscle weight from aged mice treated with vehicle (blue) or PGDHi (red) for 1 month. (**H**) Representative oil-immersion confocal images of young and aged postsynaptic AChRs stained with α-BTX. Arrowheads indicate BTX-labeled AChRs in endolysosomal vesicles. Scale bars, 20 μm. (**I**) Quantification of endolysosomal vesicles associated with AChRs in young, aged vehicle-treated (blue), and aged PGDHi-treated (red) mice ($n = 4$ young, $n = 6$ aged vehicle-treated, and $n = 5$ aged PGDHi-treated mice). Data are presented as means ± SEM in (C) to (G) and (I). (C to G) Unpaired t test. (I) One-way ANOVA with Tukey's multiple comparisons test. *$P < 0.05$, ***$P < 0.001$, and ****$P < 0.0001$.

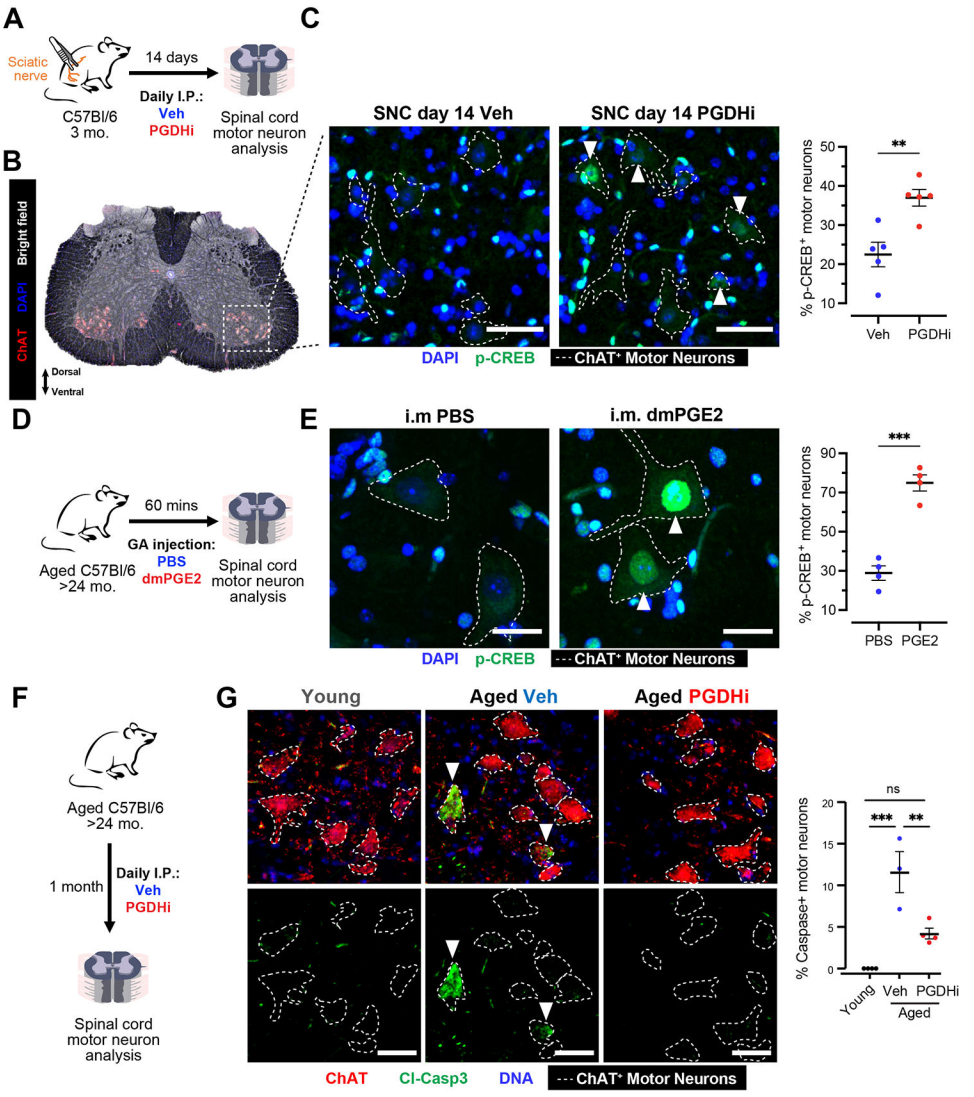

Fig. 7. PGE2 elicits CREB activation and survival of lumbar motor neurons.

(**A**) Experimental scheme. Mice were injected daily intraperitoneally with PGDHi or vehicle after SNC and analyzed 14 dpi to assess lumbar motor neuron response. (**B**) Representative images of a transverse section of lumbar spinal cord stained with TrueBlack (bright field), overlaid with immunofluorescence staining for ChAT (red) in ventral horn motor neurons. Nuclei are stained with DAPI (blue). (**C**) Representative images and quantification of p-CREB (green) in nuclei of ChAT^{+} motor neurons (outlined on the basis of ChAT staining in fig. S8B) in transverse sections of lumbar spinal cord 14 days after SNC injury in vehicle- and PGDHi-treated mice (n = 5 each). Scale bars, 50 μm. Unpaired t test. (**D**) Experimental scheme. Aged mice were injected intramuscularly with PBS or dimethyl-prostaglandin E2 (dmPGE2) into the GA muscles to assess lumbar motor neuron response. (**E**) Representative images and quantification of p-CREB (green) in nuclei of ChAT^{+} motor neurons (outlined based on ChAT staining in fig. S8C) in transverse sections of lumbar spinal cord 1 hour after intramuscular (i.m.) injection of PBS or PGE2 into the GA of aged mice (24 months; n = 4 each). Scale bars, 25 μm. Unpaired t test. (**F**) Experimental scheme. Aged mice

were injected daily intraperitoneally with PGDHi or vehicle for 30 days to assess lumbar motor neuron response. (**G**) Representative images of ChAT (red) and Cl-Casp3 (green) in transverse sections of lumbar spinal cord from aged mice treated for 1 month with vehicle and PGDHi. Scale bars, 50 μm. Quantification of Cl-Casp3 positivity in $ChAT^{+}$ motor neurons in young ($n = 4$) and aged mice treated for 1 month with vehicle ($n = 3$) and PGDHi ($n = 4$). One-way ANOVA with Tukey's multiple comparisons test. Data are presented as means ± SEM in (C), (E), and (G). $^{**}P < 0.01$ and $^{***}P < 0.001$.